Materials and Structures, 1995, **28**, 450–458

Modelling drying shrinkage of cement paste and mortar Part 1. Structural models from nanometres to millimetres

DALE P. BENTZ[1], DANIEL A. QUENARD[2], VERONIQUE BAROGHEL-BOUNY[3], EDWARD J. GARBOCZI[1], HAMLIN M. JENNINGS[4]

[1] *Building Materials Division, National Institute of Standards and Technology, Gaithersburg, MD 20899, USA*
[2] *Centre Scientifique et Technique du Bâtiment, 38400 Saint-Martin d'Hères, France*
[3] *Laboratoire Central des Ponts et Chaussées, 75732 Paris, France*
[4] *Departments of Civil Engineering and Materials Science and Engineering, Northwestern University, Evanston, IL 60208, USA*

The nanostructure of calcium silicate hydrate (C-S-H) gel contributes to many physical properties of concrete, including the important engineering properties of creep and shrinkage. A set of structural models for this gel and computational techniques for their validation have been developed. The basic nanostructure of C-S-H is conceived as a self-similar agglomeration of spherical particles at two levels (diameters of 5 nm and 40 nm). Computational techniques are presented for simulating transmission electron microscopy images and computing sorption characteristics of the model nanostructures. Agreement with available experimental data is reasonable. The development of these nanostructural models is a first step in a multi-scale approach to computing the drying shrinkage of model cement-based materials. Such an approach will provide a better understanding of the relationships between microstructure and the shrinkage behaviour of these systems.

1. INTRODUCTION

While the drying shrinkage of concrete has been studied extensively, it is only recently that the need to relate microstructure to basic mechanisms has been emphasized [1–3]. From the authors' perspective, this step is seen as a necessity to aid in the validation of proposed mechanisms [4, 5] and for the development of material parameter based models to predict the shrinkage behaviour of structures. A major obstacle in elucidating these relationships is the wide range of scales existing between the observed shrinkage behaviour of 1 m^3 samples of concrete and the controlling physical processes (capillary condensation, etc.) occurring at or below the nanometre level in the 'gel' phase of the cement paste. For many of the size levels in between these two extremes, the material exhibits a heterogeneous structure which may need to be accounted for either explicitly or statistically in models of shrinkage behaviour. Examples of this heterogeneity include: the cement paste microstructure at the micrometre level which consists of unhydrated cement particles, gel, crystalline hydration products such as calcium hydroxide, and porosity, and the concrete itself at the scale of millimetres, consisting of cement paste, aggregates, and air voids.

Currently, computational capabilities do not exist which would allow one to consider directly the heterogeneity present at these different scales in a single model. Thus, the use of a multi-scale approach [2, 6] is necessitated. Here, a number of structural models are developed, each at a different scale. The property information computed at one scale is used as input into the next higher scale. For example, properties computed from a model of the nanostructure of the calcium silicate hydrate (C-S-H) gel can be used as input for the gel phase of a micrometre level cement paste model. Likewise, the properties computed here can be input into a millimetre level model of mortar or concrete. Because a complete set of models has not yet been developed and validated, an unanswered question remains as to the extent to which properties computed for a phase at one level can be homogenized at a higher level. For example, can the properties of the C-S-H gel be considered homogeneous at the micrometre level or are there differences between the inner and outer products that must be taken into account [2]? One example where inhomogeneity must be considered explicitly is the cement paste near an aggregate (the interfacial zone) in conventional concrete, which has a different microstructure and properties from the bulk cement paste [6]. Here, the paste heterogeneity can be accounted for explicitly in performance models [7], as the concrete must be considered as a three-phase material [8], even when air voids are ignored.

At each scale of interest, different analytical techniques for probing the structure of a material are available. At the micrometre level, pore structure can be measured indirectly using mercury intrusion porosimetry and the microstructure can be directly observed also using scanning electron microscopy (SEM) [9] or x-ray microtomography [10]. At the nanometre level, the structure of the C-S-H gel can be inferred from sorption experiments [11]. At this level, small angle neutron scattering (SANS) is a useful nondestructive evaluation technique, providing a scattering profile representing a

0025-5432/95

Fourier transform of the sample nanostructure [12, 13] which can be analysed to obtain pore surface area directly. Still, structural interpretations of these measurements can be confirmed only partially by high resolution transmission electron microscopy (TEM) [14], with a resolution limit of the order of tens of nanometres, whereas the actual structure exists at levels of nanometres and tenths of nanometres. Atomic force microscopy (AFM) may offer one means of observing the gel structure directly at the nanometre level.

Our goal in the present work is to develop a set of computational tools which allows the generation of structures at a variety of scales and the subsequent calculations of properties and production of computer images in order to validate the structural models against experimental measurements. Because structural models of cement paste at the micrometre level have been developed previously [2, 6, 15], in this paper, we concentrate on the nanometre level structure of the C-S-H gel, with the ultimate goal of linking to the existing models for cement paste. We will consider agglomeration of nanometre scale spherical particles as the basic model for the structure of C-S-H at this level. Although not considered here, one might also be interested in the 'crystalline' or layer structure of the C-S-H within each spherical particle. While no definitely proven structure has been determined at this level, it should be noted that progress is being made towards accurately identifying this crystalline structure [16, 17], which could be important for understanding certain aspects of drying shrinkage, such as the irreversible shrinkage observed during a first drying [18]. Once a reasonable set of structural models has been developed, one can proceed to investigate shrinkage mechanisms using finite element techniques [19].

2. COMPUTATIONAL TECHNIQUES

2.1 Nanostructure

The basic model for the structure of C-S-H at the nanometre level is based on a hard core–soft shell representation [20]. The individual C-S-H particles are represented as spheres, each consisting of an impenetrable hard core surrounded by a concentric soft shell which can overlap freely both the hard cores and the soft shells of other particles. While any size distribution of particles can be matched using the model [21], for simplicity, we will limit our representations to monosize particles. The particles will be placed in a three-dimensional cubic box using periodic boundary conditions such that a desired interparticle porosity is achieved. For C-S-H, some overlap of these ideal spherical particles is necessary to achieve the desired low porosities (lower than dense sphere packings), as is also indicated in observing TEM images of the gel [14].

This continuum representation can then be digitized at various resolutions for the production of images and computation of properties as described below. For example, a 3-D system of side 25 nm can be digitized into a 3D array of 200^3 pixels where each pixel is of side 0.125 nm. For this model, the size of the individual spheres must be chosen; here, it will be based on an existing interpretation of SANS data from the literature [12], as detailed in the results section.

For our model C-S-H structure, a two-level (macro/micro) 'self-similar' structure will be generated to represent the C-S-H particles between scales of 1 nm and 100 nm. The C-S-H will be considered as a system of 'large' (tens of nanometres) spherical agglomerates, each composed of many smaller (nanometre size) spherical particles. Such a self-similar multi-scale model is not uncommon for gel-like materials, as it serves as a conceptual basis for structural models of aerogels [22]. Evidence for such a structure for C-S-H is provided by SANS data and TEM images [12–14].

2.2 Image production

For comparison against images of real structures, it is quite useful to be able to produce simulated TEM and other types of images of structures existing only within the computer. To simulate a TEM image, one selects a given thickness section of the three-dimensional continuum structure, digitizes it into a 3D image (cubic array, $J(x, y, z)$, typically 256 on a side), and simply sets the intensity of each pixel in the simulated TEM image according to

$$I(x, y) = f(x)^* \sum_z (1 - J(x, y, z))$$

where $J(x, y, z)$ is equal to 1 for pixels digitized as solids and 0 for pixels digitized as porosity and $f(x)$ is an arbitrary weighting function taken as equal to one in the examples provided in this paper. To compare against real TEM images, it is of interest to superimpose the sub-nanometre level texture of the gel onto an image generated at the macro level. This can be achieved approximately by generating a TEM at the tenths of a nanometre scale, rescaling it to match the scale of the macro image, and using a maximum operation (at each pixel, the resultant image is composed of the maximum grey level present in the two component images) to combine the two images.

One can also simulate atomic force microscopy images using these same principles. Here, after the 3D digitization, the 2D image intensities are computed as

$$I(x, y) = C - \min\{z{:}J(x, y, z) = 1\}$$

where $\min\{z{:}J(x, y, z) = 1\}$ indicates the depth in the sample at which solid material is first encountered and the value is subtracted from C (e.g., 255 for an 8-bit grey level representation) to obtain the desired effect that solids closer to the surface in contact with the AFM tip ($z = 0$) are brighter. Fig. 1 shows a simulated AFM image for the micro-level structure of the model C-S-H. The ability to produce such images allows a direct comparison

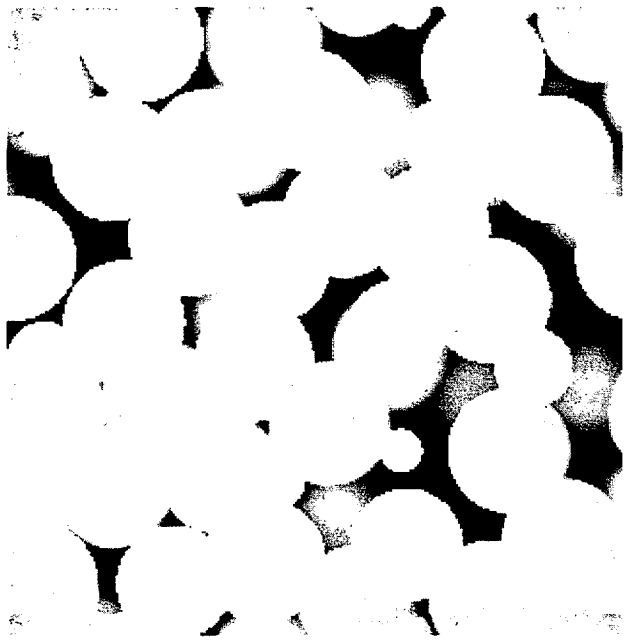

Fig. 1 Simulated AFM image of the micro-level model C-S-H structure: complete image is 25 nm × 25 nm.

to be made between the computer model and the real material, as will be illustrated for TEM images in the results section.

2.3 Physical measurements (sorption and molecular probes)

Much indirect information on the nanopore structure of C-S-H has been generated from sorption-type experiments. Simulation of two types of experiment will be described here: generation of an adsorption–desorption isotherm and the measurement of pore volume using molecules of different sizes. Both algorithms are based on purely geometrical analyses of the 3D digitized representation of the solid–pore structure.

The algorithm for adsorption–desorption in two dimensions has been described previously [23]. Here, two modifications are employed to extend the model to three dimensions and consider surface adsorption. The conversion between the physical process of capillary condensation and a geometrical algorithm is achieved based on the Kelvin–Laplace equation, which relates the vapour pressure to a characteristic pore size via

$$\ln(P/P_0) = (2V_m\gamma)/(rRT)$$

where P is the vapour pressure of a droplet of radius r, γ is a liquid surface tension, V_m its molar volume, T is absolute temperature, R is the universal gas constant, and P_0 is the vapour pressure for a planar ($r = \infty$) surface under standard conditions. For water at a temperature of 25°C, upon substitution, one obtains

$$P/P_0 = \exp(-1.0553/r)$$

where r is in nanometres.

During adsorption, the condition for capillary condensation at a given relative humidity (RH) is that the radius of a pore has to be lower than the radius computed from the Kelvin–Laplace equation. Thus, for a given radius r_c one can remove from consideration all the locations in the pore system where a digitized sphere of radius r_c can be located without overlapping any solid pixels. Any pore space remaining would indicate the volumes occupied by adsorbed water at this RH. For desorption, this geometrical constraint is augmented by a connectivity analysis. A capillary pore can empty only when its size equals or exceeds the Kelvin–Laplace radius and it is connected to the exterior of the sample by a pathway consisting exclusively of the same size or larger 'empty' pores. This is similar to the connectivity analysis by a critical sphere introduced recently by Thovert *et al.* [24], and is also the basis of the Katz–Thompson theory for relating permeability to pore structure [25].

It must be noted that assuming a spherical structure for condensed water is only an approximation, as two radii of curvature are present in 3D so that a variety of ellipsoidal shapes are possible, a problem not encountered in the 2D model [23]. Also, for the C-S-H model, we are applying this equation at very low RH (<40%), where its validity is known to be questionable. Recognizing these limitations, it is nevertheless useful to compare computed with measured isotherms.

Because the C-S-H structure has a large surface area (about 400 $m^2\ g^{-1}$ D-dried C-S-H [26]), surface adsorption is also an important consideration. For hardened cement paste, the statistical thickness (defined as the adsorbed volume divided by the BET surface area) t of an adsorbed layer of water as a function of RH has been measured and fitted to an equation of the form [27]

$$t(\text{nm}) = 0.395 - 0.189\ln(-\ln(P/P_0)).$$

This adsorbed water must be considered in the capillary condensation process. In a digitized representation of a structure, application of an adsorbed layer n pixels thick can be achieved by n dilations [28] of the solid structure before the examination of capillary condensation effects. Non-integer pixel adsorption thicknesses x can be approximated by executing the integer value of x, int(x), dilations and adding the value obtained by multiplying the exposed surface area remaining after capillary condensation analysis by the factor [x − int(x)].

Also of interest for C-S-H gel is the accessibility of the pore structure to molecules of different sizes. In the literature, for example, different porosities have been measured by water, nitrogen, methanol, isopropanol, and cyclohexane [29]. The determination of the porosity available to a given size molecule is computed in two steps. First, an algorithm similar to the desorption described earlier is used to determine all locations in the structure which are accessible to a sphere of a given radius. Second, digitized spheres of this radius are packed into the volume determined in step 1 with the condition that the spheres cannot overlap one another. The porosity is measured as the number of spheres placed

Table 1 Details of micro-/macro-level models for C-S-H

Model	System size (side)	Resolution per pixel (200^3)	Particle diameter	Hard core	Soft shell	Number of particles	Porosity
Micro	25 nm	0.125 nm	5 nm	3.7 nm	1.3 nm	212	22.3%
Macro	250 nm	1.25 nm	40 nm	22 nm	18 nm	675	7.63%

multiplied by the volume of a single sphere. Using digitized spheres to represent molecular shape is once again an approximation. Furthermore, the molecular shapes could be altered significantly in very small pores due to intermolecular forces, etc.

This algorithm is applied directly to the micro-level model of the C-S-H. For the macro-level model, as the smallest pores are larger than the diameter of the largest molecule of interest, it is assumed that all of the porosity will be measured. The same assumption is made for the capillary pores existing in a hardened cement paste.

3. RESULTS

Based on the interpretation of SANS data provided in [12], diameters of 5 and 40 nm were selected for the spheres in the micro and macro-level models of C-S-H, respectively. More recent SANS results [30] have confirmed this 5 nm diameter, suggesting a particle diameter on the order of 6 nm which is achieved very early in the cement hydration and changes very little thereafter. Also, Jennings and Tennis arrived at a diameter of 5.4 nm for the C-S-H gel particles based on a simple analysis of the density and surface area of the gel [26]. The value of 40 nm chosen for the macro-level model is also based on SANS data [12], but could vary with sample age and composition, as some TEM images suggest a value closer to 100 nm [14].

It is also necessary to decide the distribution of porosity between these two levels. The total internal porosity of the C-S-H gel was set at 28%, a generally accepted value for this parameter. The macro-level model was assigned a porosity of 7.6% with the solids in this model being assigned a porosity of 22.3% at the micro-level, for a total porosity of 28.2%. This distribution of porosity was chosen such that the volume of pores in the micro-level would equal that indicated by measured sorption isotherms [31]. Details of the two models are summarized in Table 1.

As described in the computational techniques section, a composite TEM image of the model C-S-H was produced. A direct comparison against a TEM image of the C-S-H gel in a tricalcium silicate (C_3S) paste [14] is provided in Fig. 2. While contrast differences exist and the macro particles are larger in the real image, the model appears to capture much of the structure of the real C-S-H at the scale presented.

By counting solid–pore interfaces in the pixel-based representation of the nanostructure of the model C-S-H,

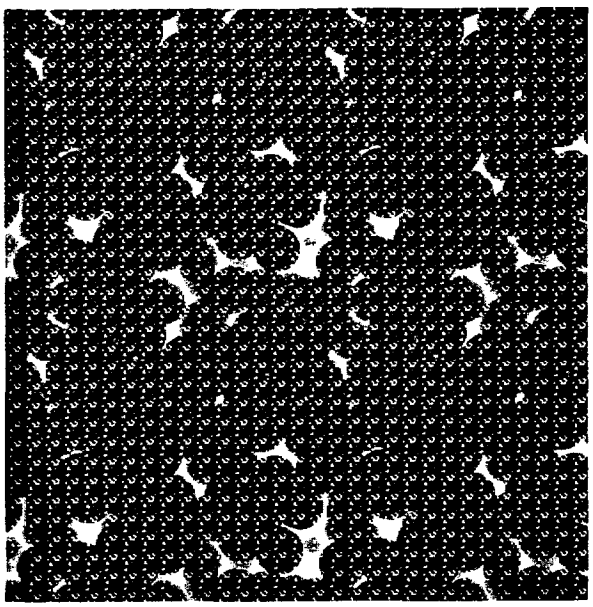

(a)

(b)

Fig. 2 (a) Simulated and (b) real TEM images of C-S-H macro-level structure: simulated image is 500 nm × 500 nm; real image is 1380 nm × 1450 nm (courtesy of Dr. R. Maggion [14]).

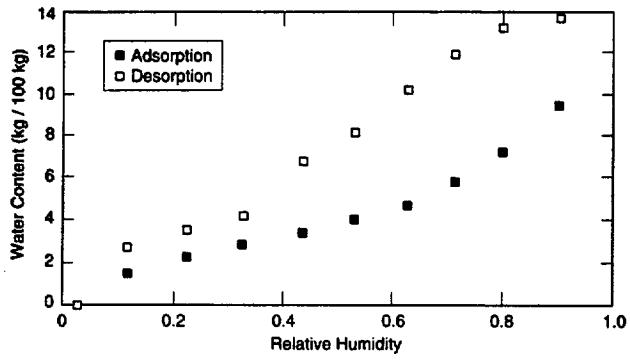

(a)

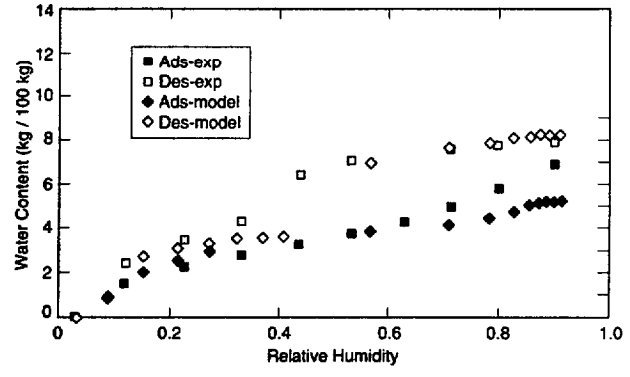

(b)

Fig. 3 Water adsorption–desorption isotherms for two hardened cement paste samples. (a) System with w/c ratio of 0.348; (b) system with water/binder ratio of 0.196 and contains 10% silica fume. Model results are compared with experimental for part (b).

one arrives at a surface area estimate of about 220 m^2 per g D-dried paste. Using water as an adsorbate, values typically presented in the literature are of the order of 200 $m^2\ g^{-1}$ [29]. The model value would be expected to be slightly higher since the 0.125 nm pixel resolution of the micro-level C-S-H model is smaller than the size of a water molecule. Thus, a value within 10% of that measured experimentally seems reasonable.

Fig. 3 presents measured sorption isotherms for two cement paste systems [31]. Several points are worth noting from these experimental curves. First, the two sets of experimental curves are practically identical for water contents below 7%. Thus, while the capillary porosities of the two samples are different (due to their different starting water-to-cement (w/c ratios), the porosities at the nano-level are quite similar. Stoichiometric calculations [32] indicate that these two samples would contain approximately the same volume fractions of C-S-H gel, which suggests that in terms of behaviour during water sorption, the C-S-H gel is identical in the two pastes. This is an interesting conclusion since it is well known that the Ca/Si molar ratio of the C-S-H gel and polymerization of the silicate ions are different with (system B) and without (system A) silica fume [16]. Thus, although the chemical structure of the gel is altered by the presence of pozzolans (silica fume, fly ash, etc.), its physical structure at the nanometre level may be the same, as suggested previously [33].

A second point of interest is the large drop in the desorption curves observed between 33% and 44% RH, particularly for system B. Based on the Kelvin–Laplace equation, this would correspond to a pore diameter between 2.0 nm and 2.5 nm. If surface adsorption is included in the calculation, one obtains a pore diameter between 2.6 nm and 3.5 nm. Similar to a threshold diameter in mercury intrusion [21, 25], this value is taken to indicate the maximum size of pores that are continuous across a volume of C-S-H gel. This means that, to traverse a volume of C-S-H, one must consider at least pores of this size and larger. If only pores larger than this are considered, the C-S-H gel is discontinuous, i.e., a sphere larger than this critical size cannot pass through the pore structure. For system B, the pronounced drop in the desorption curve in this RH range is due to the existence of isolated capillary pores which can undergo desorption (empty) only when the surrounding C-S-H gel can do the same.

For system B, as shown in Fig. 3, a comparison was made between sorption isotherms computed for the model C-S-H and those measured on the cement paste. Here, the following assumptions were made: the paste contains 58% C-S-H by volume, 7% capillary porosity, and has a specific gravity of 2.29. While not an exact match, the agreement between experimental and model curves is promising. The difference in the adsorption branches at high RH is due to the presence of the small isolated capillary pores (0.01–0.1 μm) in the paste which are not considered in a model based strictly on the C-S-H. Thus, the ultimate value achieved in the adsorption branch for the model is below that observed experimentally. In this very low water-to-binder ratio paste with silica fume one would expect these pores to be isolated, as the capillary porosity would become disconnected early in the hydration process [32]. Thus, for the desorption branch, we have included this capillary porosity (7% or 3 kg per 100 kg) and assumed that these isolated capillary pores are detected (empty) only when the surrounding macro-level C-S-H structure empties, between RH's of 41% and 57% for the model structure. This range partially overlaps the RH range of 33–44% observed experimentally.

Jennings and Tennis have measured the degree of hydration and pore volume accessible to a series of molecules (H_2O, CH_3OH, C_3H_7OH, and C_6H_{12}) for a cement paste at five w/c ratios [26]. Their results are shown in Fig. 4a. To compare these results with those for the model, estimates of the volumes of C-S-H and capillary pores present in each sample are needed. To obtain these, the assumption was made that the cement paste is pure C_3S, the main component of Portland cement. Knowing the w/c ratio and measured degree of hydration [26], the volumes needed can be calculated for a C_3S paste [32]. While the exact sizes of the real molecules used on the abscissa in Fig. 4a are somewhat

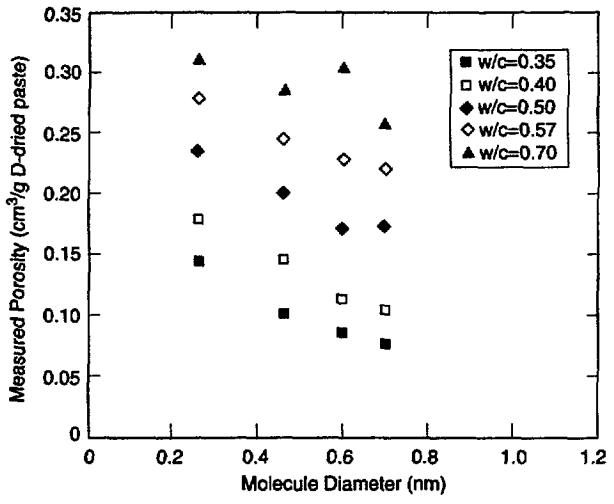

(a)

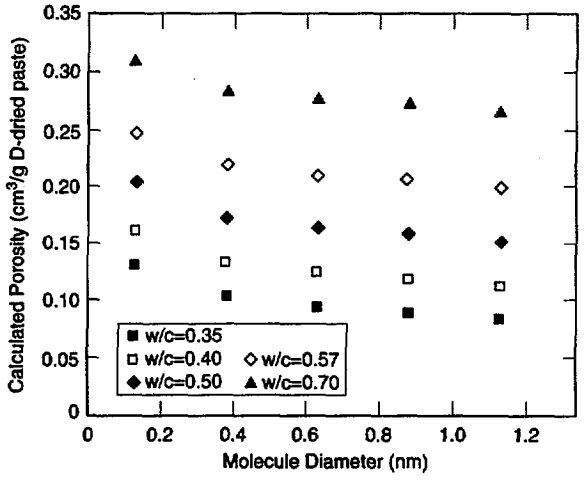

(b)

Fig. 4 Comparison of (a) experimental and (b) model pore volumes versus molecule size: from left to right, experimental points are for water, methanol, isopropanol, and cyclohexane.

questionable [29], the model results shown in Fig. 4b do indicate the same trends as those observed experimentally. Once again, measurements computed on the model structures are considered to exhibit reasonable agreement with those determined experimentally for the real material.

4. DISCUSSION

The goal of the present research has been to present a methodology and computational techniques for developing and validating a structural model for C-S-H at the nanometre level. While further refinements are always possible, the basic model presented here seems to portray accurately many of the observed characteristics of the C-S-H gel. Examples of refinements which could be explored include using a size distribution of C-S-H particles at the macro- and/or micro-levels or using ellipsoidal particles instead of spheres. This would be fairly straightforward as the computational techniques for both of these modifications now exist [21, 34]. Here, we have assumed that the porosity distribution between macro- and micro-level models is constant. While the data in Fig. 3 support this hypothesis, other data over a larger range of *w/c* ratios seem to indicate that this distribution may vary somewhat with *w/c* ratio [2].

Using the present model for C-S-H, and previously existing models for cement paste and mortar, one can proceed to compute the shrinkage behaviour of cement-based materials via finite element techniques. At each scale of interest, one must know the elastic properties and shrinkage of each phase [2]. For C_3S paste, a computational study of the elastic behaviour of simulated paste microstructure based on these techniques has exhibited good agreement with experimental measurements [35]. There, however, it was necessary to calibrate the elastic properties of the C-S-H gel and C_3S via experimental data. (The elastic properties of calcium hydroxide were available for direct input.) With an accurate representation of the nanostructure of C-S-H, one will perhaps be able to calculate directly its elastic properties for input into the micrometre level cement paste model. As an example of this, the conductivity of the macro-level C-S-H gel has been computed by mapping the microstructure into a network of resistors [36, 37]. The computed formation factor of 200 is in excellent agreement with values of 100–400 previously obtained in calibrating a micrometre level cement paste model against impedance spectroscopy [38] and chloride ion diffusion data [36].

Fig. 5 outlines a proposed plan for combining these multi-scale models to investigate the shrinkage of cement paste and mortar. Assuming that the elastic properties of each phase are available at each level and that the drying shrinkage is due primarily to capillary-type forces, one can proceed as follows. Although the following discussion is limited to capillary forces, one should be able to incorporate equally other stresses such as those due to changes in surface free energy or disjoining pressure [4, 5], since a complete 3D representation of structure is available.

For a given RH, using the techniques described herein, one can compute the locations of all the capillary condensed water in a set of structural models. It is worth noting that at a fixed RH, these locations may be different during drying from self-desiccation [39]. For the former, one can utilize the desorption algorithm to compute the water locations, while in the latter case the adsorption algorithm may be more appropriate from a theoretical standpoint [39], although experimentally measured moisture contents and internal relative humidities achieved during self-desiccation have been observed to lie mainly on desorption isotherm curves [40]. At the micro C-S-H level, one can specify capillary stresses (based on the critical pore radius fixed by the RH [41]) at all solid–liquid interfaces and determine the bulk shrinkage of the structure using a finite element code. At the macro-level, this bulk shrinkage will be present in

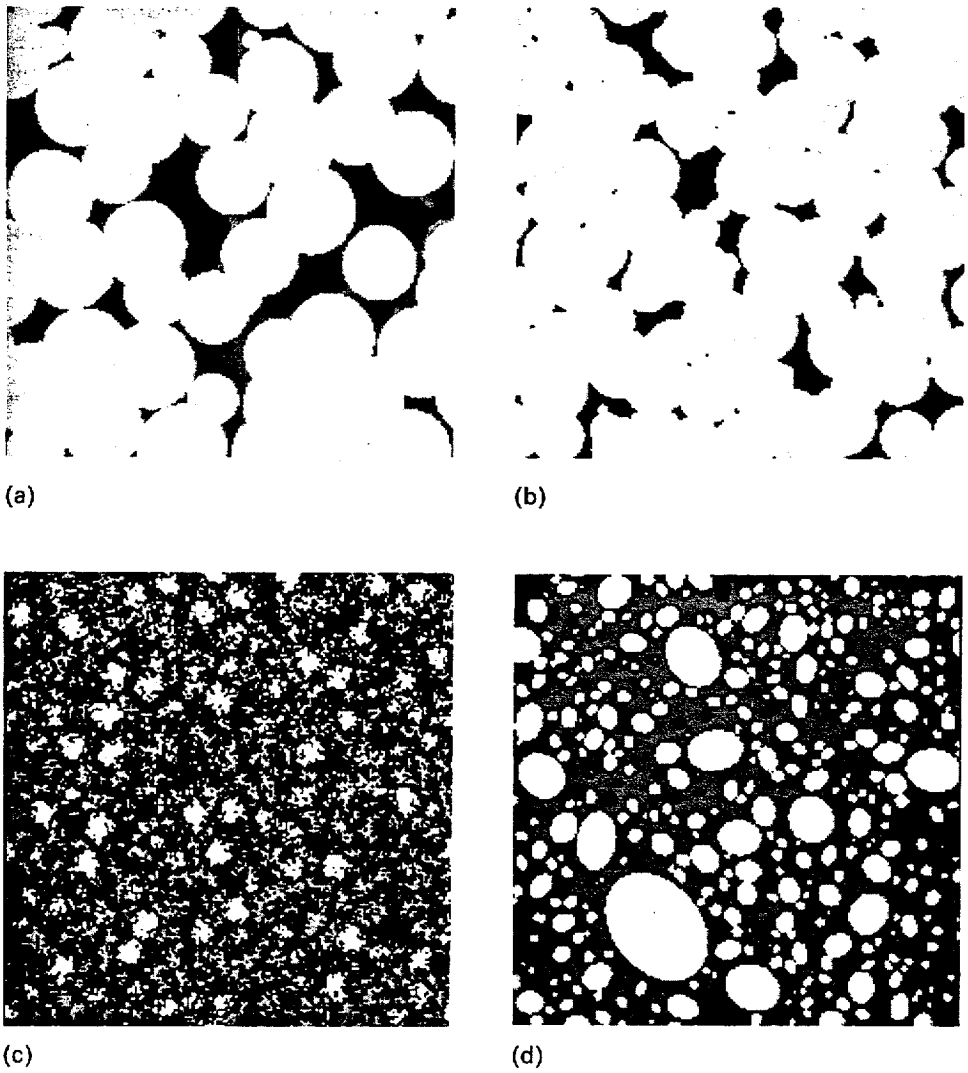

Fig. 5 Two-dimensional images from three-dimensional structural models for cement-based materials at different scales and proposed manner to model shrinkage at each level. (a) C-S-H at micro-level (25 nm × 25 nm): white = solid; black = porosity; grey = water (RH = 9%, desorption); capillary forces at liquid/solid interfaces. (b) C-S-H at macro-level (250 mm × 250 mm): white = solid; black = porosity; capillary forces at interfaces; bulk shrinkage of micro C-S-H. (c) Cement paste at micrometre level (200 μm × 200 μm): white = C_3S; light grey = calcium hydroxide; dark grey = C-S-H gel; black = capillary porosity; capillary forces at interfaces; bulk shrinkage of C-S-H gel. (d) Mortar at millimetre level (10 mm × 10 mm): white = sand; grey = bulk cement paste; black = interfacial zone paste; bulk shrinkage of cement paste as a function of paste type and location in specimen.

each of the C-S-H particles in addition to the capillary forces again present at solid–liquid interfaces. At this level, one can compute the bulk shrinkage of the C-S-H gel which will be input into the cement paste model. Next, one can compute the bulk shrinkage of the cement paste at the micrometre level due to the shrinkage of the C-S-H gel that it contains and the capillary stresses in any water-filled capillary pores. After computing the bulk shrinkage of a cement paste microstructure at a *w/c* ratio and degree of hydration of interest, one can finally proceed to compute the shrinkage in a mortar sample. Here, as indicated in the figure, one may need to consider the interfacial zone paste and bulk cement paste separately, as their shrinkage characteristics may differ [42]. Additionally, it is at this level that gradients in moisture content may become important so that the shrinkage of each cement paste pixel will be a function of its spatial location and the specimen geometry. All of these complications can be addressed systematically within the framework of the multi-scale digital-image-based modelling approach described previously [6].

This methodology does not consider stress relief due to microcracking and creep, but will indicate to what extent the non-shrinkage behaviour of sand grains and unhydrated cement reduces the bulk shrinkage of a paste or mortar sample. Experimentally, a factor of ten reduction has been observed in comparing the shrinkage of micrometre size samples observed in an environmental SEM with that commonly measured in large scale shrinkage tests [2]. It is hoped that having such a detailed representation of structure at all scales of importance, along with a set of computational tools to compute

properties, will provide a sound scientific basis for understanding better the relationships between microstructure and drying shrinkage in cement-based materials.

5. CONCLUSION

A multi-scale approach for modelling the structure of cement-based materials has been presented. At each scale of interest, a critical exercise is the validation of the structural models against measured experimental data. Here, this validation has been demonstrated for nanometre level models of the structure of C-S-H gel by comparison against TEM images and measured sorption characteristics. The development of a complete set of representative structural models at all scales of interest should aid greatly in understanding the structure–property relationships present in this complex class of materials.

ACKNOWLEDGEMENT

D.B. would like to thank the Centre International des Etudiants et Stagiaires (C.I.E.S.) for a grant which allowed this research to be pursued during a six-month stay at the Centre Scientifique et Technique du Bâtiment (CSTB) in Grenoble, France.

REFERENCES

1. Xi, Y. and Jennings, H. M., 'Relationships between microstructure and creep and shrinkage of cement paste', in 'Materials Science of Concrete III', edited by J. P. Skalny and S. Mindess (American Ceramic Society, Westerville, OH, 1992) pp. 37–69.
2. Jennings, H. M. and Xi, Y., 'Microstructurally based mechanisms for modelling shrinkage of cement paste at multiple levels', in 'Creep and Shrinkage of Concrete', edited by Z. P. Bazant and I. Carol (E&F Spon, London, 1993) pp. 85–102.
3. Hua, C., (Analyses et modélisation de retrait d'autodessiccation de la pâte de ciment durcissante', Ph.D. thesis, L'école National des Ponts et Chaussées. Paris, France, 1992.
4. Ferraris, C. F. and Wittmann, F. H., 'Shrinkage mechanisms of hardened cement paste', *Cement Concr. Res.* **17** (1987) 453–464.
5. Hansen, W., 'Drying shrinkage mechanisms in Portland cement paste', *J. Amer. Ceram. Soc.* **70** (1987) 323–328.
6. Bentz, D. P., Schlangen, E. and Garboczi, E. J., 'Computer simulation of interfacial zone microstructure and its effect on the properties of cement-based composites', in 'Materials Science of Concrete IV', edited by J. P. Skalny and S. Mindess (American Ceramic Society, Westerville, OH, 1994) pp. 155–199.
7. Schlangen, E., 'Experimental and numerical analysis of fracture processes in concrete', Ph.D. thesis, Delft University of Technology, The Netherlands, 1993.
8. Nilsen, A. U. and Monteiro, P. J. M., 'Concrete: a three phase material', *Cement Concr. Res.* **23** (1993) 147–151.
9. Scrivener, K. L., 'The microstructure of concrete', in 'Materials Science of Concrete I', edited by J. P. Skalny (American Ceramic Society, Westerville, OH, 1989) pp. 127–161.
10. Schwartz, L. M., Auzerais, F., Dunsmuir, J., Martys, N., Bentz, D. P. and Torquato, S., 'Transport and diffusion in three-dimensional composite media', *Physica* A, 'Proceedings of the 3rd International Meeting of Electrical, Transport, and Optical Properties of Inhomogeneous Materials' (1993).
11. Baroghel-Bouny, V. and Chaussadent, T., 'Caractérisation de la texture d'un béton durci à partir des isothermes de sorption de vapeur d'eau', 'Bulletin de Liaison des Laboratoires des Ponts et Chaussées' **187** (1993) 69–75.
12. Allen, A. J., Oberthur, R. C., Pearson, D., Schofield, P. and Wilding, C. R., 'Development of the fine porosity and gel structure of hydrating cement', *Phil. Mag.* B **56** (1987) 263–288.
13. Allen, A. J., Baston, A. H. and Wilding, C. R., 'Small angle neutron scattering studies of pore and gel structures, diffusivity, permeability, and damage effects', 'Symposium Proceedings', Vol. 137 (Materials Research Society, 1989) pp. 119–125.
14. Maggion, R., 'Etude de l'évolution microtextural de pâtes de silicate tricalcique hydraté', Ph.D. thesis, Université d'Orléans, Orléans, France, 1992.
15. Garboczi, E. J. and Bentz, D. P., 'Computer-based models of microstructure and properties of cement-based materials', in 9th International Cement Chemistry Congress, New Delhi, India, 1992, Vol. VI, pp. 3–15.
16. Taylor, H. F. W., 'Nanostructure of C-S-H current status', *Adv. Cement-Based Mater.* **1** (1993) 38–46.
17. Nonat, A., 'Interactions between chemical evolution (hydration) and physical evolution (setting) in the case of tricalcium silicate', *Mater. Struct.* **27** (1994) 187–195.
18. Helmuth, R. A. and Turk, D. H., 'The reversible and irreversible drying shrinkage of hardened Portland cement and tricalcium silicate paste', Research Department Bulletin 215 (Portland Cement Association, 1967).
19. Garboczi, E. J., Bentz, D. P. and Quenard, D. A., 'Modelling capillary controlled drying shrinkage in porous materials: application to porous Vycor glass', *J. Amer. Ceram. Soc.* (1995) in press.
20. Torquato, S., 'Bulk properties of two-phase disordered media. 1. Cluster expansion for the effective dielectric constant of dispersions of penetrable spheres', *J. chem. Phys.* **81** (1984) 5079–5088.
21. Winslow, D. N., Cohen, M. D., Bentz, D. P., Snyder, K. A., and Garboczi, E. J., 'Percolation and pore structure in mortars and concretes', *Cement Concr. Res.* **24** (1994) 25–37.
22. Special issue on Proceedings of the 3rd International Symposium on Aerogels, *J. of Non-Crystalline Solids* **145** (1992) 1–259.
23. Quenard, D. A., Bentz, D. P., and Garboczi, E. J., 'Capillary condensation, hysteresis, and image analysis', in 'Drying '92', edited by A. S. Mudjumar, Pt. A (Elsevier, London, 1992) pp. 253–262.
24. Thovert, J. F., Salles, S., and Adler, P. M., 'Computerized characterization of the geometry of real porous media: their discretization, analysis, and interpretation', *J. Microsc.* **170** (1993) 65–79.
25. Katz A. J. and Thompson, A. H., 'Quantitative prediction of permeability in porous rock', *Phys. Rev.* B **34** (1986) 8179; 'Prediction of rock electrical conductivity from mercury injection measurements', *J. geophys. Res.* **92** (1987) 599.

26. Jennings, H. M. and Tennis, P. D., 'Model for the developing microstructure in Portland cement paste', *J. Amer. Ceram. Soc.*, **77** (1994) 3161–3172.
27. Badmann, R., Stockhausen, N. and Setzer, M. J., 'The statistical thickness and the chemical potential of adsorbed water films', *J. Colloid Interface Sci.* **82** (1981) 534–542.
28. Serra, J., 'Image Analysis and Mathematical Morphology', Vol. I (Academic Press, London, 1982).
29. Mikhail, R. Sh. and Selim, S. A., 'Adsorption of organic vapors in relation to the pore structures of hardened Portland cement pastes', Symposium on the Structure of Portland Cement Paste and Concrete, Highway Research Board Special Report 90, (National Academy of Engineering, 1966) pp. 123–132.
30. Eichhorn, F., Haussler, F. and Baumbach, H., 'Structural studies on hydrating cement paste', *J. Physique* IV **3** (1993) 369–372.
31. Baroghel-Bouny, V., 'Caractérisation microstructurale et hydrique de pâtes de ciment et des bétons ordinaires et à très hautes performances', Ph.D. thesis, Ecole National des Ponts et Chaussées, Paris, France, June 1994.
32. Bentz, D. P. and Garboczi, E. J., 'Percolation of phases in a three-dimensional cement paste microstructural model', *Cement Concr. Res.* **21** (1991) 325–344.
33. Atlassi, E., 'Some moisture sorption properties of silica fume mortar', in '4th Canmet/ACI International Conference on Fly Ash, Silica Fume, Slag, and Natural Pozzolans in Concrete', Vol. 2 (American Concrete Institute, Detroit, MI, 1992) pp. 903–930.
34. Hwang, J. T. and Hagwood, C., 'Necessary and sufficient conditions for two ellipsoids to have an intersection', unpublished.
35. Garboczi, E. J. and Day, A. R., 'Computer simulation computation of the elastic moduli of C_3S cement paste', unpublished.
36. Garboczi, E. J. and Bentz, D. P., 'Computer simulation of the diffusivity of cement-based materials', *J. Mater. Sci.* **27** (1992) 2083–2092.
37. Day, A. R. and Garboczi, E. J., 'DC conductivity and elastic moduli of a model interpenetrating composite', unpublished.
38. Coverdale, R. T., Christensen, B. J., Jennings, H. M., Mason, T. O., Bentz, D. P. and Garboczi, E. J., 'Interpretation of impedance spectroscopy of cement paste via computer modelling. Part I: Bulk conductivity and offset resistance', *J. Mater. Sci.* **30** (1995) 712–719.
39. Buil, M., 'Contribution à l'étude de retrait de la pâte de ciment durcissante', *Rapport de Recherche des Laboratoires des Ponts et Chaussées*, No. 92, Dec. 1979.
40. Nilsson, L. O., private communication, 1994.
41. Scherer, G. W., 'Theory of drying', *J. Amer. Ceram. Soc.* **73** (1990) 3–14.
42. Sujata, K., Xi, Y. and Jennings, H. M., 'Interfacial shrinkage in mortars', *Ibid.*, in press.

RESUME

Modélisation du retrait au séchage de la pâte de ciment et du mortier. 1ère Partie. Modèles structuraux, des nanomètres aux millimètres

Beaucoup de propriétés physiques du béton, y compris le fluage et le retrait à l'échelle macroscopique, dépendent de la structure à l'échelle nanométrique du gel formé par les hydrates de silicate de calcium (C-S-H). Une série de modèles structuraux du gel, ainsi que des simulations par ordinateur pour vérifier leur validité, ont été développés. La nanostructure de C-S-H est conçue comme une agglomération auto-similaire de particules sphériques à deux échelles: diamètres de 5 et 40 nm. Les techniques numériques sont développées pour simuler la transmission électronique à balayage ainsi que l'adsorption sur la structure modèle. Les simulations sont en bon accord avec les résultats expérimentaux disponibles. Le développement de ces modèles structuraux à l'échelle nanométrique est une première étape vers une approche multi-échelle visant à simuler le retrait par séchage des matériaux à base de ciment. Une telle approche fournira une meilleure compréhension des relations qui existent entre la microstructure et le comportement au retrait de ces systèmes.